Wave equation-based reflection tomography of the 1992 Landers earthquake area

Xueyuan Huang[1,2], Dinghui Yang[1], Ping Tong[3], José Badal[4], and Qinya Liu[2]

[1]Department of Mathematical Sciences, Tsinghua University, Beijing, China, [2]Department of Physics, University of Toronto, Toronto, Ontario, Canada, [3]Department of Geophysics, Stanford University, Stanford, California, USA, [4]Physics of the Earth, Sciences B, University of Zaragoza, Zaragoza, Spain

Abstract In the framework of a recent wave equation-based traveltime seismic tomography, we show that incorporating Moho-reflected phases (*PmP* and *SmS*) in addition to the direct *P* and *S* phases can significantly increase tomography resolution in the lower crust and this may provide additional evidence to resolve important tectonic issues. To highlight the resolving power of the new strategy, we apply it in the region around the 1992 Landers earthquake ($M_w = 7.3$) in Southern California using seismic arrivals from local earthquakes, obtaining 3-D high-resolution *P* and *S* wave crustal velocity models and Poisson's ratio structures. In the upper crust, our method confirmed features that had been previously found. However, in the middle-to-lower crust, we found low-velocity anomalies on the southeastern section of the San Jacinto Fault and high V_p and low V_s structures to the west of the Big Bear earthquake, which may be related to upwelling of partial melt from the mantle.

1. Introduction

The development of seismic imaging techniques based upon solving full wave equations has become a topic of great research interest during the past several decades [e.g., *Luo and Schuster*, 1991; *Tromp et al.*, 2005; *Fichtner et al.*, 2009; *Chen et al.*, 2007; *Tape et al.*, 2009; *Tong et al.*, 2014a]. As one of the attempts, *Tong et al.* [2014a] developed a wave equation-based traveltime seismic tomography (WETST) method, which naturally takes into account the finite-frequency effects of seismic waves and accurately captures the interaction between seismic waves and complex velocity structure. Since only the traveltime information is considered, WETST assumes that acoustic seismic waves propagate in a 2-D vertical plane passing through the source and receiver with *P* or *S* velocity for numerical efficiency but inverts for 3-D velocity model of the study region. The relatively low computational costs allow this 2-D-3-D seismic tomography method to use as many seismic records as the conventional ray-based tomographic methods. To show the validity of the WETST method, *Tong et al.* [2014b] chose the 1992 Landers earthquake area in Southern California as the test field.

Southern California is one of the most seismically active regions in the world [*Tian et al.*, 2007]. Tens of thousands of earthquakes have been recorded by the Southern California Seismic Network (SCSN), which provides us abundant data to explore the seismic structures of this region. Following the pioneering seismic tomography work of *Aki and Lee* [1976], many studies have been conducted to explore the subsurface structure in Southern California [e.g., *Dziewonski et al.*, 1977; *Zhao and Kanamori*, 1993; *Zhao et al.*, 2005; *Tape et al.*, 2009, 2010], revealing structural heterogeneities in the crust and upper mantle of this region [e.g., *Lin et al.*, 2007; *Tape et al.*, 2010; *Tong et al.*, 2014b]. The results provided by *Tong et al.* [2014a] are consistent with the other studies, indicating the validity of the WETST method in real applications. However, only the first *P* and/or *S* wave arrivals were used in most tomographic inversions concerning the Southern California region [e.g., *Lin et al.*, 2007; *Allam and Ben-Zion*, 2012], including the one of *Tong et al.* [2014b]. Since the crustal earthquakes mainly occurred in the upper and middle crust (Figure 1b), the tomographic resolution of the lower crust is generally poor [*Zhao et al.*, 2005; *Lin et al.*, 2007; *Tong et al.*, 2014b]. Adding Moho-reflected phases (such as *PmP*, *pPmP*, *SmS*, and *sSmS*) to tomographic inversion is an efficient way to improve the data coverage in the lower crust. *Zhao et al.* [2005] conducted a two-station tomographic inversion for the Landers earthquake area with first *S*, *SmS*, and *sSmS* arrivals. *Xia et al.* [2007] mapped out tomographic images of the crust under active arc volcanoes in the central part of Northeast Japan with *P* and *PmP* arrivals. These studies demonstrate that reflected phases are able to improve significantly the resolution of the lower crust.
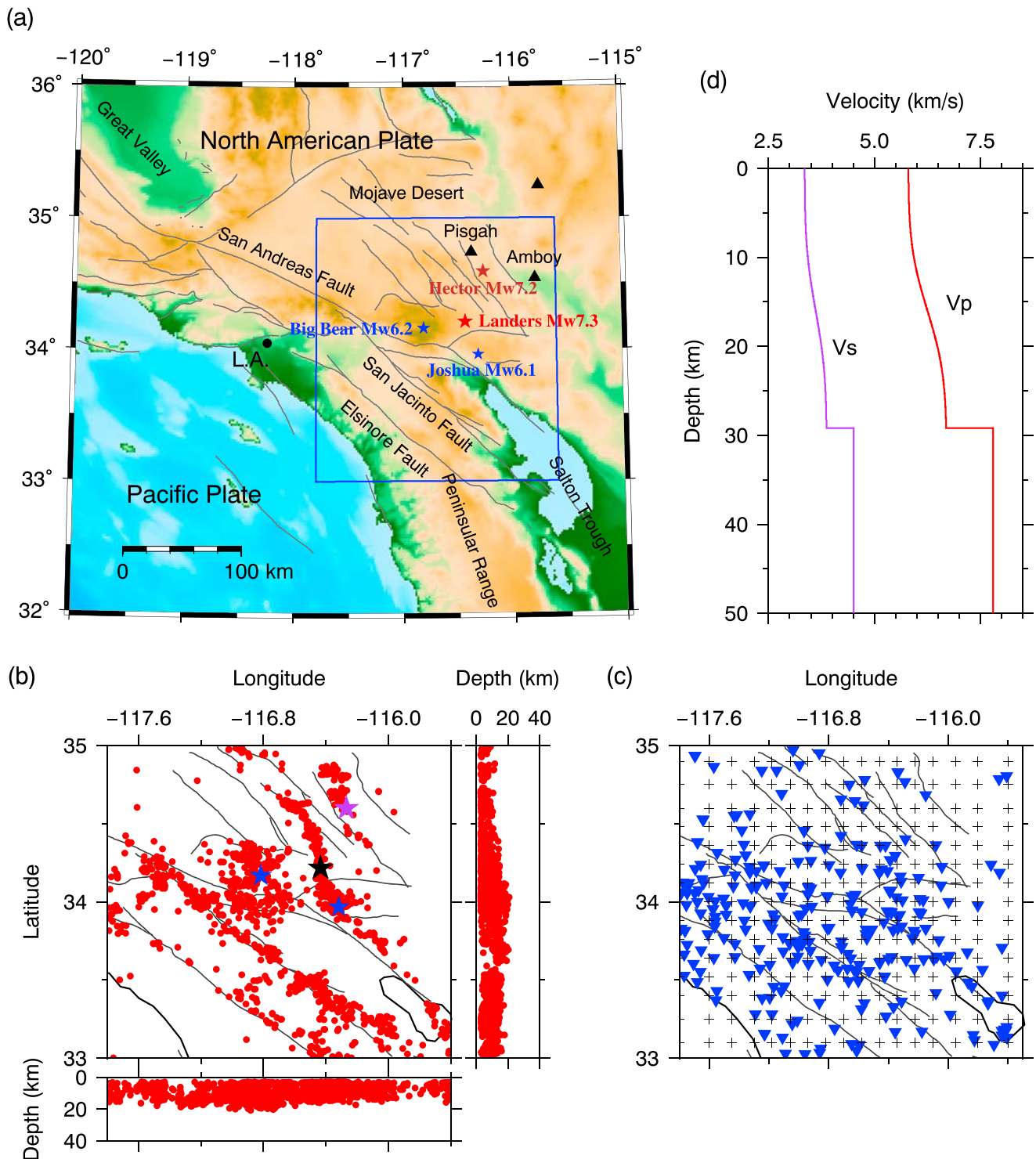
Figure 1. (a) The tectonic background of Southern California. Major faults are shown in grey curves. The blue box indicates the present study area. The stars show the epicenters of the 1992 Landers earthquake($M_w = 7.3$) and three relatively large earthquakes. (b) The hypocenter distribution of the earthquakes (red dots) used in this study. The stars denote the relatively large earthquakes. (c) Spatial distribution of the 276 seismic stations (blue reverse triangles). The grey crosses represent the inversion grid nodes. (d) 1-D smooth velocity model used as the initial velocity model for the tomographic inversion. The red line shows the *P* wave velocity model, and the purple line shows the *S* wave velocity model.

Given that previous tomographic studies in Southern California are mainly based on ray theory and neglect the influence of off-ray structure on the observables, in this study we intend to explore to which extent the subsurface images can be improved when both first arrivals and Moho-reflected phases are used with the wave equation-based traveltime seismic tomography method [*Tong et al.*, 2014a]. To this end, the 1992 Landers earthquake area is again chosen as the study field. The Landers earthquake, which has a moment magnitude of 7.3, occurred on 28 June 1992 at the depth of 7.0 km in the southeast of the Mojave Desert (Figure 1a). The SCSN recorded more than 10,000 aftershocks in 1992 [*Hauksson et al.*, 1993]. Several relatively large earthquakes, such as the Joshua Tree earthquake (M_w 6.1), the Big Bear earthquake (M_w 6.2), and the Hector Mine earthquake (M_w 7.1) (see Figure 1a), are considered to be related to this earthquake [*Parsons and Dreger*, 2000]. We expect that the tomographic results obtained by inverting the Moho-reflected phases (*PmP* and *SmS*) and first arrival phases (*P* and *S*) with the wave equation-based reflection tomography method can further help us to understand the seismic heterogeneity and earthquake dynamics of the Lander earthquake area in Southern California.

2. Data and Model Parameterization

We use seismic traveltime data of local earthquakes recorded by the SCSN during the period from 1 January 1992 to 31 December 2013 (Figure 1c). The selection of first arrivals is based on the following five criteria: (1) the magnitudes of the selected events are within the range [2.5, 4.0]; (2) only events with more than 20 *P* and *S* arrivals are chosen; (3) the difference between the observed traveltime and the prediction time calculated for a 1-D reference model should be within a reasonable range (no more than 1.0 s and 1.5 s for *P* and *S* arrivals, respectively) to reduce the influence of picking errors; (4) seismic records with epicentral distance no more than 95 km and events with focal depth greater than 3.0 km are chosen; (5) the research area is divided into blocks whose size is 2.5 km × 2.5 km × 2.0 km and only one event with the maximum number of records is selected in each block. The reasons for these criteria are presented in the Supporting Information. As a result, 23,537 *P* arrivals and 12,462 *S* arrivals from 473 local earthquakes were selected.

Since the focal depths of most crustal earthquakes are shallower than 20 km in the study area, sensitivity kernels of the first arrivals generally cover only the upper and middle crust (Figure 2b). To improve the resolution of the lower crust, we manually pick the Moho-reflected phases (i.e., *PmP* and *SmS*) and combine them with the direct *P* and *S* picks in tomographic inversion (Figure 2c). However, it is challenging to pick a massive number of later seismic phases from high-frequency seismograms generated by local earthquakes [*Zhao et al.*, 2005]. Figure 2a shows examples of band-pass-filtered (0.1–7.5 Hz) vertical-component seismograms recorded by various stations for a particular event. Similar to the discussions in *Nakajima et al.* [2002], the Moho-reflected phases have three main features in the study region, namely, (1) they can be only observed in an epicentral distance range [30 km, 100 km] and may be interfered by other phases. (2) The amplitudes of the Moho-reflected phases are large and sometimes larger than the first arrivals, which suggests that these phases are generated at boundaries (i.e., Moho) with sharp velocity contrast or at high impedance interface. (3) The arrival time difference between *SmS* and *S* is about 1.7 times of that between *PmP* and *P*. Considering these features, we picked the arrival times of the Moho-reflected phases based on the following criteria. (1) The magnitudes of the selected events should be within the range [3.0, 4.0]. (2) Only the seismic records with epicentral distances within [37.0 km, 95.0 km] were considered. (3) The raw seismograms were band-pass filtered in the interval [0.1 Hz, 7.5 Hz]. As a result, 4558 *PmP* arrivals from 1236 local earthquakes and 4717 *SmS* arrivals from 1296 local earthquakes were hand picked. As shown in Figures 1b and 1c, the distributions of the selected earthquakes and seismic stations are generally evenly distributed in the study area.

For tomographic inversion, we set up 3-D inversion grid at the depths of 1, 5, 10, 15, 21, 28, and 40 km (Figure 1c). The horizontal intervals are 0.12° at the central portion and 0.15° near the boundaries of the research domain (Figure 1c). Previous works suggest that the Moho topography has a significant effect on the tomographic images, especially in an area like Southern California with large lateral variations of the Moho depth [*Zhu and Kanamori*, 2000; *Tian et al.*, 2007; *Zhao et al.*, 2005]. Therefore, the starting model is built by adding the Moho topography variation obtained by [*Zhu and Kanamori*, 2000] to the 1-D model shown in Figure 1d (with a flat Moho at 29.2 km). Other parameters used in this study are given in the Supporting Information.
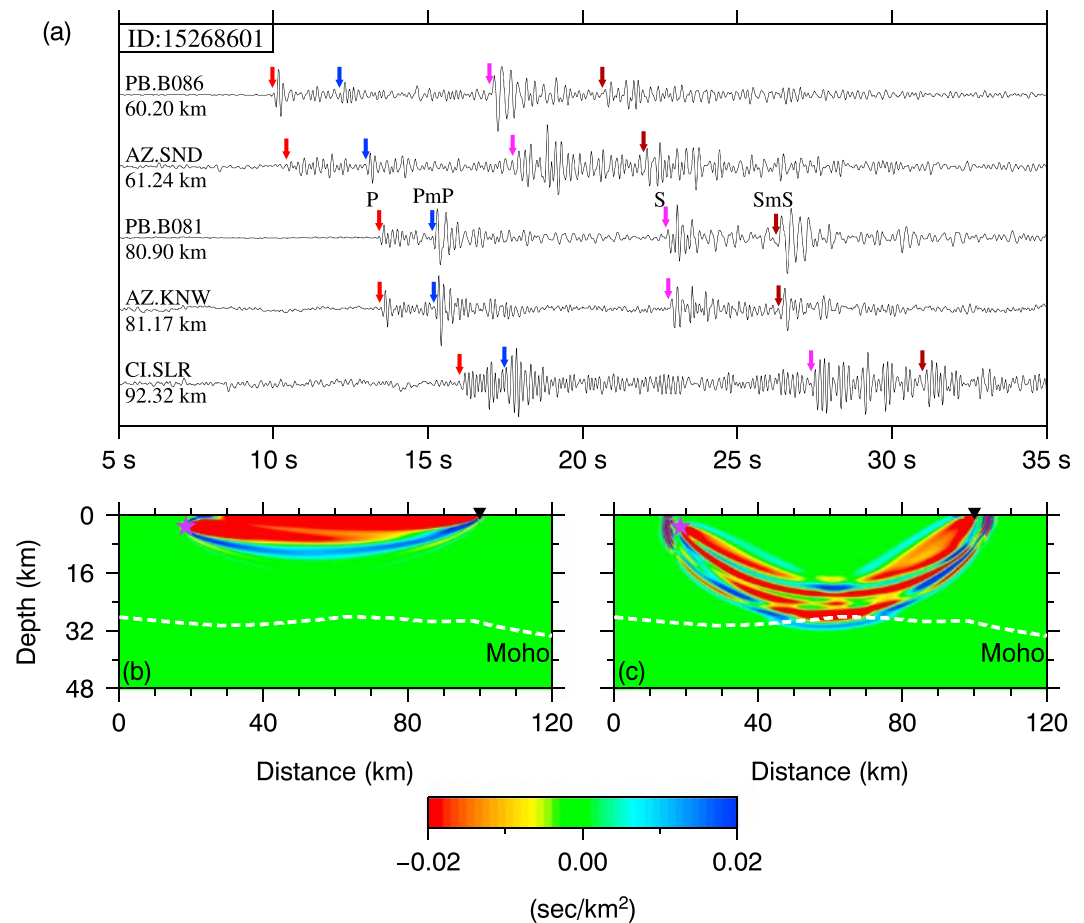
Figure 2. (a) The vertical-component seismograms generated by the earthquake ID 15268601, filtered between 0.1 Hz and 7.5 Hz. The names of seismic stations (such as PB.B086) and the corresponding epicentral distances are specified. The arrows indicate the arrival times of the seismic phases of *P*, *PmP*, *S*, and *SmS*, respectively. (b) Traveltime sensitivity kernel for the first arrival phase corresponding to the direct *P* wave of the third seismogram in Figure 2a. (c) Traveltime sensitivity kernel corresponding to the *PmP* phase of the third seismogram in Figure 2a. In each case, the purple star and black reverse triangles represent the source and stations, respectively. The dashed white line denotes the Moho discontinuity obtained by *Zhu and Kanamori* [2000].

3. Resolution Tests

We first conduct checkerboard resolution tests to investigate the resolving ability of the WETST method with the selected seismic data. A checkerboard model with alternating positive and negative velocity perturbations of 6% is assigned to the 3-D inversion grid nodes. Figure 3 shows the inversion results of checkerboard tests for *P* wave velocity (V_p) at six representative depths after only one iteration. Figures 3a–3f show the results based only on first *P* arrivals, while Figures 3g–3l are the inversion results after using both the first *P* and Moho-reflected *P* (*PmP*) arrivals. Generally speaking, the checkerboard patterns at the depths less than 20 km (Figures 3a–3d and 3g–3j) are well recovered in the explored area of the Landers earthquake for both cases. However, at depths deeper than 20 km (Figures 3e, 3f, 3k, and 3l), the checkerboard structure is poorly recovered with only the first *P* arrivals. With the addition of *PmP* phases, the resolution in the lower crust is greatly improved (Figures 3e, 3f, 3k, and 3l). The inversion results provided by checkerboard tests for *S* wave velocity (V_s) are very similar (Figure S1 in the Supporting Information).

Table 1 shows quantitatively the structural similarity (SSIM) indices defined by *Tong et al.* [2011] between the recovered *P* or *S* velocity models and the input checkerboard models at seven layers. As discussed in *Tong et al.* [2014b], the inverted model is better recovered when the SSIM index is close to 1.0. It can be observed that the SSIM indices are above 0.75 at the depths less than 21.0 km regardless of whether Moho-reflected phases are used or not. When both Moho-reflected phases and first arrival phases are used, the values of SSIM indices of
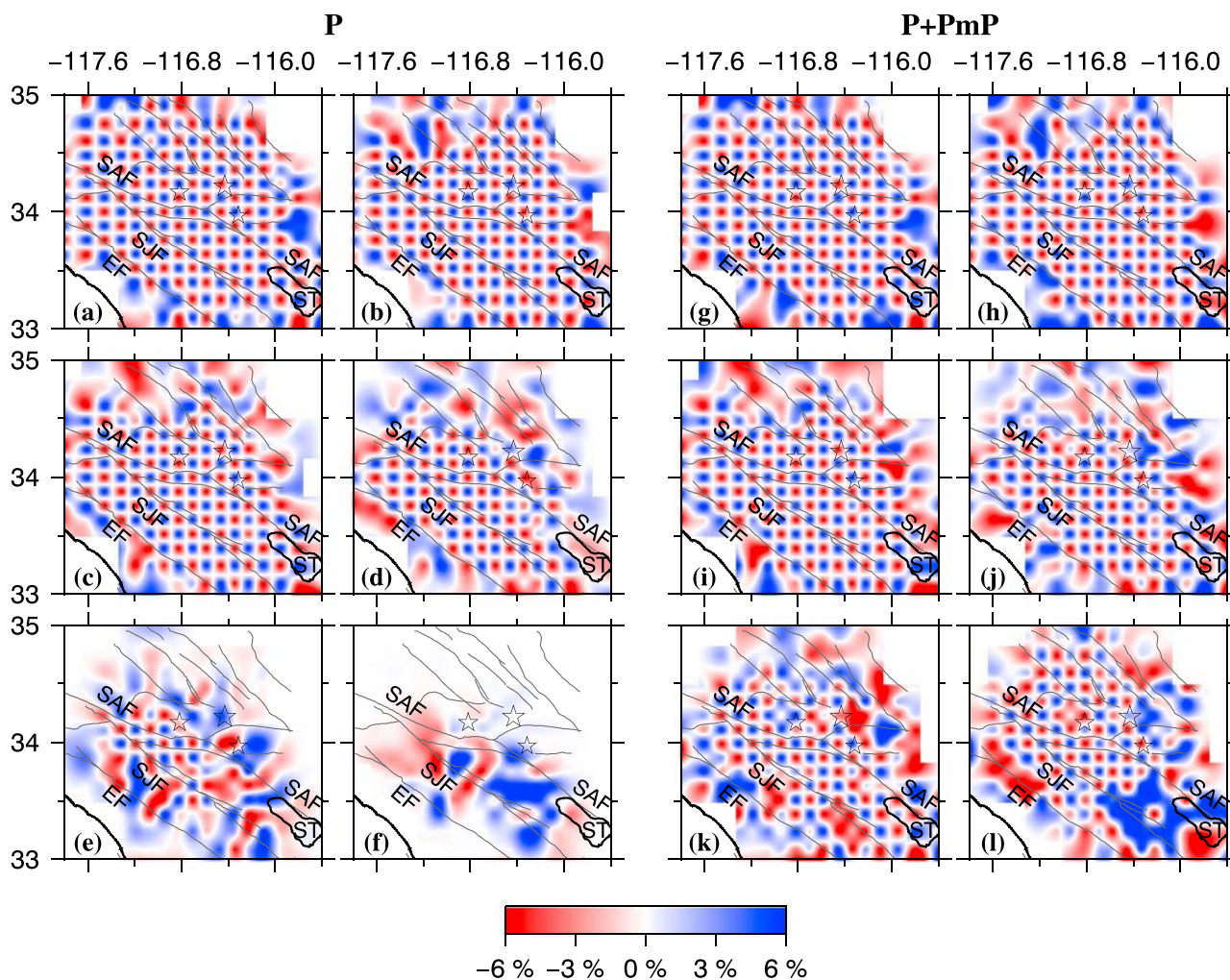
Figure 3. Inversion results obtained from the checkerboard tests for *P* wave velocity structures at six representative depth layers (1.0, 5.0, 10.0, 15.0, 21.0, and 28.0 km). (a–f) The results based on first *P* arrivals only. (g–l) The results obtained by combining first *P* and *PmP* arrivals. Blue and red colors represent high- and low-velocity perturbations, respectively. The stars denote the epicenter locations of the Landers, Joshua Tree, and Big Bear earthquakes.

recovered models are above 0.77 at depths no more than 28 km, while the SSIM indices with only first arrivals are less than 0.6 even at depth of 21.0 km. This confirms that the Moho-reflected phases can help to improve the resolution of lower crust seismic tomography. The SSIM indices at 40.0 km depth are around 0.5, implying a significant decreasing of the resolution in the uppermost mantle [*Tong et al.*, 2014b]. Considering the picking errors, off plane effects, noises, and other grid scales for comparison, the results of checkerboard tests with added random noises and different grid scales are given in the Supporting Information (Figures S3–S8). These results of the checkerboard resolution tests indicate that the tomographic results in the crust obtained by inverting all the arrival time data are reliable and can be used for further interpretation [*Tong et al.*, 2014b].

Table 1. The Structural Similarity Indices (SSIM) Between the Checkerboard Models and the Inverted Results at Seven Typical Depths for *P* and *S* Velocity Checkerboard Resolution Tests When Moho-Reflected Phases are Included or Not

Depth	1.0 km	5.0 km	10.0 km	15.0 km	21.0 km	28.0 km	40.0 km
Only *P*	0.8980	0.8684	0.8199	0.7414	0.5598	0.4854	0.5009
PmP + *P*	0.8930	0.8685	0.8199	0.7768	0.7863	0.8569	0.4873
Only *S*	0.8838	0.8681	0.8093	0.7676	0.5836	0.4837	0.5019
SmS + *S*	0.8840	0.8075	0.8084	0.7896	0.7751	0.8571	0.5168

4. Results and Discussion

We iteratively update the crustal velocity models of the Landers earthquake area by inverting all the picked first and Moho-reflected arrivals (the traveltime residuals over three iterations are shown in Figure S12). Restricted by the data coverage, only the crustal tomographic results are discussed in this study. In general, the tomographic results of the upper and middle crust are consistent with previous studies for overlapping research areas (see Figures 4, S10, and S11) [e.g., *Zhao and Kanamori*, 1993; *Zhou*, 2004; *Tian et al.*, 2007; *Tape et al.*, 2010; *Lin et al.*, 2010; *Allam and Ben-Zion*, 2012; *Tong et al.*, 2014b]. Strong lateral heterogeneities (up to ±8%) are revealed in the crust [*Lin et al.*, 2007; *Tape et al.*, 2009; *Tong et al.*, 2014b], which reflect complex compositional, structural, and petrological variations [*Tong et al.*, 2014b]. The inverted velocity models are correlated with the surface geology in the upper crust [*Lin*, 2013; *Tong et al.*, 2014b]. Along the main faults in this area, such as the San Andreas Fault and the San Jacinto Fault, prominent low-velocity anomalies exist, which may have resulted from the fractured rocks within the faulting zones [*Tian et al.*, 2007]. The Los Angeles basin is observed as a relatively low-velocity region because of the thick sedimentary materials [*Lin et al.*, 2010]. The mountain ranges, such as the Peninsular Ranges in the study area and the Santa Rosa-San Jacinto Mountains, present relatively high-velocity anomalies at shallow depths. The high-velocity anomalies that extend even to middle crust may reflect the roots of these mountains [*Tian et al.*, 2007].

Figure 4 shows three vertical velocity cross sections of the research area from the free surface to 40 km depth for V_p, V_s, and Poisson's ratio σ structures. It can be observed that the three large earthquakes along the north-south profile AB are all located around or in regions dominated by high velocity and low Poisson's ratio anomalies (Figures 4a–4c). Most seismicities along the profile are the aftershocks of the Landers earthquake. Profile CD along the San Jacinto Fault (SJF) is generally dominated by a low velocity and high Poisson's ratio layer in the upper crust (0–7 km) [*Tong et al.*, 2014b] and a high velocity and low Poisson's ratio structure in the middle crust. Seismicity along this profile is rather dense [*Lin*, 2013], and most of them extend in the high velocity and low Poisson's ratio region [*Tong et al.*, 2014b] or near the boundaries of high- and low-velocity anomalies, which can be interpreted as the seismogenic layer. Similar features can be observed around the hypocenters of the Big Bear and Landers earthquakes. The distribution of earthquakes along these profiles clearly shows that seismic activity is related to velocity structures therein [*Lin et al.*, 2007] and mostly distributed in or near areas with high velocity and low Poisson's ratio, which is consistent with the conclusions of previous studies that velocity and Poisson's ratio structures can change significantly around the hypocenters of the relatively large earthquakes [e.g., *Lees and Nicholson*, 1993; *Tong et al.*, 2014b]. The high velocities observed in or near rupture zones in the upper crust around Landers earthquake faulting zone are generally considered to be brittle, which may also indicate instability in the geological structures [*Zhao and Kanamori*, 1993, 1995; *Lin et al.*, 2007], and are always capable of generating earthquakes [*Zhao and Kanamori*, 1995]. These results indicate the validity of the wave equation-based reflection tomography and that the tomographic images can be used to study crustal structures and dynamic processes of the area.

Some other structural anomalies are also revealed along the three profiles. Beneath the hypocenters of the Joshua Tree and Landers earthquakes, prominent high-velocity anomalies exist surrounding a small weak low-velocity patch in the middle crust. The small low-velocity patch, combining with studies of dynamic simulations of the Landers earthquake and the Joshua Tree earthquake [e.g., *Hough et al.*, 1994; *Olsen et al.*, 1997], may be formed by the ruptures of the two earthquakes. The high-velocity region, with a cap of low-velocity anomalies in the uppermost crust (0–5 km), extends from the middle crust to the uppermost mantle (see ellipses in Figures 4a and 4b). On both sides of the high-velocity anomaly, significant low-velocity anomalies can be observed in the lower crust. The low-velocity anomaly on the left and the low velocity and high Poisson's ratio anomalies in the lower crust along the SJF (Figures 4d and 4e)in the southeastern section close to Salton Trough are considered to be fluids derived from magma intrusion that extend in SW-NE direction from the magmatic intrusion zone in the southwest of the Salton sea [*Hussein et al.*, 2012; *Tong et al.*, 2014b]. The above mentioned high velocity in Figures 4a and 4b may indicate the boundary of the fluid-filled area, and its pattern is consistent with low Bouguer gravity anomaly distribution [*Hussein et al.*, 2012]. *Tong et al.* [2014b] only reported the low-velocity anomalies, since their tomographic results have less satisfactory recovery below 21.0 km. In the present study, structures are well recovered down to the depth of 28.0 km, which makes the lower crustal anomalies much more clear. Along the profile EF a high velocity, low Poisson's ratio anomaly is visible in the middle crust close to the hypocenter of the Landers main shock (Figures 4a–4c and 4g–4i). In the lower crust, however, unlike the tomographic results of *Tong et al.* [2014b] between the SAF and the hypocenter of the Big Bear earthquake, a dome-shaped anomaly with high V_p and low V_s can
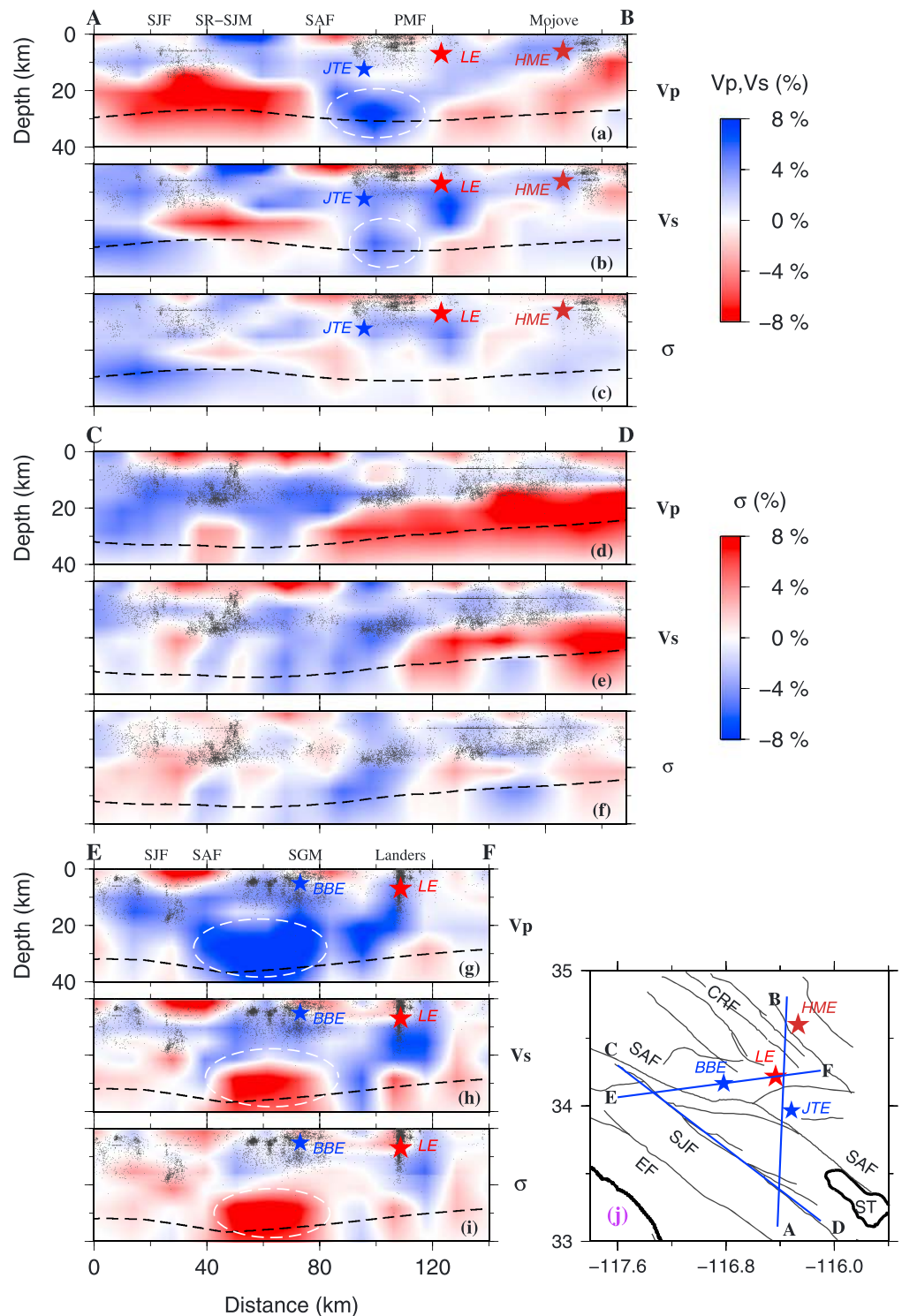
Figure 4. Vertical cross sections of V_p, V_s, and Poisson's ratio σ images along profiles (a–c) AB, (d–f) CD, and (g–i) EF as indicated on the (j) inset map. Red color denotes low velocity and high Poisson's ratio, while blue color shows high velocity and low Poisson's ratio. The grey dots represent all events with magnitudes greater than 1.5 between 1 January 1992 and 31 December 2013, located within 1.0 km width along the profiles without any screening and selection. The stars are hypocenters of the Landers earthquake (LE), Joshua Tree earthquake (JTE), Big Bear earthquake (BBE), and Hector Mine earthquake (HME). The dashed lines represent the Moho discontinuity. Abbreviations: SJF, San Jacinto fault; SR-SJM, Santa Rosa-San Jacinto Mountains; SAF, San Andreas fault; PMF, Pinto Mountain fault; Mojave, Mojave Desert; SGM, San Gorgonio Mountain; CRF, Camp Rock fault; EF, Elsinore fault; ST, Salton Trough.

be seen accompanied of high Poisson ratio (Figures 4h and 4i). Previous works suggested the possible existence of the relict Farallon-subducted slab in the mantle under these anomalies [e.g., *Jacobson et al.*, 1996; *Saleeby*, 2003], and significant low-velocity anomalies were discovered just above the relict slab in the uppermost mantle, which are considered to be formed by upwelling of asthenospheric partially melted driven by the relict subduction [*Tian et al.*, 2007]. The high V_p and low V_s anomalies discovered in this study, underplated by the low-velocity anomalies, might be due to these causes.

These results benefit from the Moho-reflected phases, which can further illuminate the middle-to-lower crust of the study area. Detailed crustal structures revealed by the results demonstrate the validity of the wave equation-based reflection tomography and its potential to improve the resolution of tomographic images with Moho-reflected phases. Though the results are improved in comparison with previous studies, it should be noted that the "2-D–3-D" approximation that ignores the off-plane effects along the wave path from the source to the receiver might introduce significant traveltime errors when the subsurface velocity model has strong heterogeneities and consequently reduce the resolution of the tomographic results. We should get rid of the 2-D-3-D approximation in our future studies when massive 3-D forward modeling becomes computationally feasible. Besides that this method relies on the acoustic assumption. If we want to further include converted phases in the tomographic inversion, the elastic wave equation should be adopted.

5. Conclusions

We use both the first arrivals and Moho-reflected phases to investigate the 1992 Landers earthquake region in Southern California with the wave equation-based reflection tomography technique. The revealed 3-D V_p, V_s, and Poisson's ratio structures are consistent with previous studies in the overlapped upper and middle crust zones, implying the validity of the wave equation-based reflection tomography method. In the lower crust, pronounced low-velocity anomalies are recovered in the southeastern segment of the San Jacinto Fault close to the Salton Trough. Between the San Andreas fault and the Pinto Mountain fault, a prominent high-velocity anomaly extends from the middle crust to the uppermost mantle. This low V_s and high Poisson's ratio anomaly may suggest the existence of crustal fluids coming from magma intrusion, which extends in SW-NE direction from the magmatic intrusion zone in the lower crust in the southwest of the Salton Trough. The high V_p anomalies on the northeast of the San Andreas fault may indicate the boundary of the crustal fluid-filled area, and its pattern is consistent with low Bouguer gravity anomaly distribution. A small low-velocity patch surrounded by high-velocity anomalies between the main shocks of the Landers and the Joshua Tree earthquakes may depict part of the rupture zone of them. An anomaly with high V_p and low V_s discovered in the lower crust to the west of the hypocenter of the Big Bear earthquake may be formed by the influence of the upwelling of partial melt asthenospheric material driven by the relict subduction. The formation of these anomalies and their dynamic processes should be further discussed in consideration that these structures may relate to upper mantle materials. The joint use of direct and Moho-reflected waves and wave equation-based seismic tomography is a useful tool to study structural heterogeneities and dynamic processes in the middle-to-lower crust.

References

Aki, K., and W. Lee (1976), Determination of the three-dimensional velocity anomalies under a seismic array using first *P* arrival times from local earthquakes: 1. A homogeneous initial model, *J. Geophys. Res.*, *81*, 4381–4399.

Allam, A. A., and Y. Ben-Zion (2012), Seismic velocity structures in the Southern California plate-boundary environment from double-difference tomography, *Geophys. J. Int.*, *190*(2), 1181–1196, doi:10.1111/j.1365-246X.2012.05544.x.

Chen, P., T. H. Jordan, and L. Zhao (2007), Full three-dimensional waveform tomography: A comparison between the scattering-integral and adjoint-wavefield methods, *Geophys. J. Int.*, *170*, 175–181.

Dziewonski, A. M., B. H. Hager, and R. J. O'Connell (1977), Large-scale heterogeneities in the lower mantle, *J. Geophys. Res.*, *82*, 239–255.

Fichtner, A., B. L. N. Kennett, H. Igel, and H. P. Bunge (2009), Full seismic waveform tomography for upper-mantle structure in the Australasian region using adjoint methods, *Geophys. J. Int.*, *179*(3), 1703–1725.

Hauksson, E., L. M. Jones, K. Hutton, and D. Eberhart-Phillips (1993), The 1992 Landers Earthquake Sequence: Seismological observations, *J. Geophys. Res. Solid Earth*, *98*(B11), 19,835–19,858, doi:10.1029/93JB02384.

Hussein, M., A. A. Velasco, L. Serpa, and D. Doser (2012), The role of fluids in promoting seismic activity in active spreading centers of the salton trough, California, USA, *Int. J. Geosci.*, *3*(2), 303–313.

Hough, S. E., Y. Benzion, and P. Leary (1994), Fault-zone waves observed at the southern Joshua-Tree earthquake rupture zone, *Bull. Seismol. Soc. Am.*, *84*(3), 761–767.

Jacobson, C. E., F. R. Oyarzabal, and G. B. Haxel (1996), Subduction and exhumation of the Pelona-Orocopia-Rand schists, Southern California, *Geology*, *24*(6), 547–550.

Lees, J. M., and C. Nicholson (1993), Three-dimensional tomography of the 1992 Southern California earthquake sequence: Constraints on dynamic earthquake rupture?, *Geology*, *21*(5), 387–390.

Lin, G. (2013), Three-dimensional seismic velocity structure and precise earthquake relocations in the salton trough, Southern California, *Bull. Seismol. Soc. Am.*, *103*(5), 2694–2708.

Lin, G., P. M. Shearer, E. Hauksson, and C. H. Thurber (2007), A three-dimensional crustal seismic velocity model for Southern California from a composite event method, *J. Geophys. Res. Solid Earth*, *112*(B11), B11306, doi:10.1029/2007JB004977.

Lin, G., C. H. Thurber, H. Zhang, E. Hauksson, P. M. Shearer, F. Waldhauser, T. M. Brocher, and J. Hardebeck (2010), A california statewide three-dimensional seismic velocity model from both absolute and differential times, *Bull. Seismol. Soc. Am.*, *100*(1), 225–240, doi:10.1785/0120090028.

Luo, Y., and G. T. Schuster (1991), Wave-equation traveltime inversion, *Geophysics*, *56*(1), 645–653.

Nakajima, J., T. Matsuzawa, and A. Hasegawa (2002), Moho depth variation in the central part of northeastern Japan estimated from reflected and converted waves, *Phys. Earth Planet. Inter.*, *130*(1–2), 31–47.

Olsen, K. B., R. Madariaga, and R. J. Archuleta (1997), Three-dimensional dynamic simulation of the 1992 Landers earthquake, *Science*, *278*(5339), 834–838, doi:10.1126/science.278.5339.834.

Parsons, T., and D. S. Dreger (2000), Static-stress impact of the 1992 Landers earthquake sequence on nucleation and slip at the site of the 1999 M = 7.1 Hector Mine earthquake, southern California, *Geophys. Res. Lett.*, *27*(13), 1949–1952, doi:10.1029/1999GL011272.

Saleeby, J. (2003), Segmentation of the Laramide slab–evidence from the Southern Sierra Nevada region, *Bull. Geol. Soc. Am.*, *115*(6), 655–668.

Tape, C., Q. Liu, A. Maggi, and J. Tromp (2009), Adjoint tomography of the Southern California crust, *Science*, *325*, 988–992.

Tape, C., Q. Liu, A. Maggi, and J. Tromp (2010), Seismic tomography of the Southern California crust based on spectral-element and adjoint methods, *Geophys. J. Int.*, *180*, 433–462.

Tian, Y., D. Zhao, and J. Teng (2007), Deep structure of Southern California, *Phys. Earth Planet. Inter.*, *165*(1–2), 93–113.

Tong, P., D. Zhao, and D. Yang (2011), Tomography of the 1995 Kobe earthquake area: Comparison of finite-frequency and ray approaches, *Geophys. J. Int.*, *187*, 278–302.

Tong, P., D. Zhao, D. Yang, X. Yang, J. Chen, and Q. Liu (2014a), Wave-equation-based travel-time seismic tomography—Part 1: Method, *Solid Earth*, *5*(2), 1151–1168, doi:10.5194/se-5-1151-2014.

Tong, P., D. Zhao, D. Yang, X. Yang, J. Chen, and Q. Liu (2014b), Wave-equation-based travel-time seismic tomography—Part 2: Application to the 1992 Landers earthquake (m_W 7.3) area, *Solid Earth*, *5*(2), 1169–1188, doi:10.5194/se-5-1169-2014.

Tromp, J., C. Tape, and Q. Liu (2005), Seismic tomography, adjoint methods, time reversal and banana-doughnut kernels, *Geophys. J. Int.*, *160*, 195–216.

Wessel, P., and W. H. F. Smith (1991), Free software helps map and display data, *EOS, Tran. AGU*, *72*, 441–446.

Xia, S., D. Zhao, X. Qiu, J. Nakajima, T. Matsuzawa, and A. Hasegawa (2007), Mapping the crustal structure under active volcanoes in central Tohoku, Japan using P and PMP data, *Geophys. Res. Lett.*, *34*(10), L10309, doi:10.1029/2007GL030026.

Zhao, D., and H. Kanamori (1993), The 1992 Landers earthquake sequence: Earthquake occurrence and structural heterogeneities, *Geophys. Res. Lett.*, *20*(11), 1083–1086, doi:10.1029/93GL01239.

Zhao, D., and H. Kanamori (1995), The 1994 Northridge Earthquake: 3-D crustal structure in the rupture zone and its relation to the aftershock locations and mechanisms, *Geophys. Res. Lett.*, *22*(7), 763–766.

Zhao, D., S. Todo, and J. Lei (2005), Local earthquake reflection tomography of the Landers aftershock area, *Earth Planet. Sci. Lett.*, *235*, 623–631.

Zhou, H.-W. (2004), Multi-scale tomography for crustal P and S velocities in Southern California, *Pure Appl. Geophys.*, *161*(2), 283–302, doi:10.1007/s00024-003-2444-7.

Zhu, L., and H. Kanamori (2000), Moho depth variation in Southern California from teleseismic receiver functions, *J. Geophys. Res.*, *105*, 2969–2980.